Knockout of transient receptor potential ankyrin 1 (TRPA1) modulates the glial phenotype and alleviates perihematomal neuroinflammation after intracerebral hemorrhage in mice via MAPK/NF-κB signaling

Min Xia[a,b,c]*, Yù-Jié Chen[a,b,c]*, Beike Chen[a,b,c], Xufang Ru[a,b,c], Jie Wang[a,d], Jie Lin[a,b,c], Xiaoqin Tang[a,b,c], Weixiang Chen[a,e], Rong Hu[a,b,c], Weina Li[a,b,c] and Hua Feng[a,b,c]

The objective is to explore the role of astrocytic transient receptor potential ankyrin 1 (TRPA1) in glial phenotype transformation in neuroinflammation after intracerebral hemorrhage (ICH). Wild-type astrocytes and TRPA1$^{-/-}$ astrocytes were subjected to 6-h hemin treatment, and the calcium ions and transcriptome sequencing were assessed. A mouse autologous blood injection ICH model was established to evaluate the proliferation and phenotypes of astrocytes and microglia around the hematoma. The neuroinflammation and behavioral performance of wild-type ICH mice and TRPA1$^{-/-}$ ICH mice were assessed. Knockout of astrocytic TRPA1 decreased calcium ions of astrocytes after hemin treatment in-vitro, and microglial and astrocytes around the hematoma proliferated after the ICH model. Furthermore, RNA-sequencing (RNA-seq), immunofluorescence, and Western blotting results showed that the activated astrocytes transformed into the A2 phenotype in TRPA1$^{-/-}$ ICH mice. The 'ameboid' microglia were observed around the hematoma in TRPA1$^{-/-}$ ICH mice. The proliferation of A2 astrocytes and 'ameboid' microglia ameliorated the neuroinflammation after ICH. The inflammatory response was reduced by inhibiting the mitogen-activated protein kinase/nuclear factor kappa-B signaling pathway, and neurologic deficits were improved in TRPA1$^{-/-}$ ICH mice compared with wild-type ICH mice. This research suggests that astrocytic TRPA1 is a new therapeutic target to rescue neuroinflammation by modulating the glial phenotype after ICH. ***NeuroReport*** **34: 81–92 Copyright © 2022 The Author(s). Published by Wolters Kluwer Health, Inc.**

NeuroReport 2023, **34**:81–92

Keywords: astrocyte, intracerebral hemorrhage, microglia, neuroinflammation, transient receptor potential ankyrin 1

[a]Department of Neurosurgery and State Key Laboratory of Trauma, Burn and Combined Injury, Southwest Hospital, Third Military Medical University (Army Medical University), [b]Chongqing Key Laboratory of Precision Neuromedicine and Neuroregenaration, Southwest Hospital, Third Military Medical University (Army Medical University), [c]Chongqing Clinical Research Center for Neurosurgery, Southwest Hospital, Third Military Medical University (Army Medical University), Chongqing, [d]Department of Neurosurgery, 970 Hospital of PLA JLSF, Yantai and [e]Department of Neurosurgery, General Hospital of Xinjiang Military Command of PLA, Urumqi, China

Correspondence to Hua Feng, MD, PhD, Department of Neurosurgery and State Key Laboratory of Trauma, Burn and Combined Injury, Southwest Hospital, Third Military Medical University (Army Medical University), 29 Gaotanyan Street, Shapingba District, Chongqing 400038, China
Tel: +(86)023 68766004; fax: +(86)023 68765922; e-mail: fenghua@tmmu.edu.cn

*Min Xia and Yù-Jié Chen contributed equally to the writing of this article.

Received 27 September 2022 **Accepted** 16 November 2022.

Introduction

Intracerebral hemorrhage (ICH) is a kind of hemorrhage in the brain parenchyma caused by the sudden rupture of tiny arteries, accounting for 10–20% of all strokes. It is the most lethal subtype of stroke, with a 1-year mortality rate of more than 50% [1]. ICH mainly occurs in the basal ganglia region, which is rich in nerve fiber bundles and many glial cells. The secondary damage caused by toxic products of hematoma, which mainly includes inflammation and oxidative stress, is considered the primary cause of the high death and disability rates of ICH patients. Significant inflammatory reactions after ICH are accompanied by the activation of proinflammatory cells and the release of proinflammatory cytokines [2]. A recent study has shown that craniotomy or minimally invasive evacuation of hematoma after ICH has no effect on the prognosis of patients within 1 year, and no specific drug can improve the prognosis of patients with ICH in clinical medication [3]. Reducing secondary brain injury in the acute stage has become the core issue of ICH treatment.

Astrocytes can deal with the neurotransmitters of neurons, affect excitability conduction, produce lactate, and provide energy for the metabolism of neurons in the central nervous system. Studies have shown the proliferation of astrocytes around hematomas in a rat ICH model. These proliferative astrocytes are generally considered to limit the expansion of the damaged area, promote inflammation, and produce reactive oxygen species (ROS) in the acute stage of ICH. A recent study has indicated that

proliferative astrocytes include proinflammatory phenotype A1 and neuroprotection phenotype A2. A1 astrocytes can cause the death of neurons and oligodendrocytes. A2 astrocytes can upregulate neurotrophic factors and play a neuroprotective role. Microglia are also activated after ICH. Initially, the activated microglia are divided into the proinflammatory M1 phenotype and the anti-inflammatory M2 phenotype [4]. However, according to recent transcriptomic studies, many newly discovered functional subsets of microglia have been found [5]. Astrocytes and microglia have a close interaction in the inflammatory response. Proinflammatory factors secreted by astrocytes can lead to the activation of microglia. IL (interleukin)-1α and tumor necrosis factor-α (TNF-α) secreted by microglia can promote reactive astrocyte proliferation [6]. Astrocytes and microglia are not usually beneficial after ICH. Therefore, regulating the phenotypic conversion of astrocytes and microglia is very important for modulating the inflammatory response.

Transient receptor potential ankyrin 1 (TRPA1) is a nonselective transmembrane cation channel with high permeability to calcium ions. This channel is known to be regulated by ROS, cold, and irritant chemicals to participate in acute inflammatory and sensory pain [7]. Recent research has shown that TRPA1 is expressed in sensory neurons, astrocytes, oligodendrocytes, and ependymal cells and plays roles in learning, emotion, memory, cognition, and social behavior [8]. The study has found that astrocytic TRPA1 can regulate resting calcium levels and GABAergic inhibitory transmission by reducing GABA transport [9]. Low-frequency and low-intensity ultrasound can activate astrocytic TRPA1 channels to regulate neuronal activity [10]. TRPA1 is also involved in many pathological processes. After traumatic brain injury, TRPA1 in sensory neurons is involved in neuroinflammation, including the activation of astrocytes and microglia [11]. Conditional knockout of astrocytic TRPA1 can alleviate demyelination in multiple sclerosis [12]. TRPA1 blockade in oligodendrocytes can reduce myelin damage after cerebral ischemia and ICH [13,14]. It is speculated that astrocytic TPRA1 may affect other natural processes after ICH.

This study aimed to explore the role of astrocytic TRPA1 in neuroinflammation after ICH and provide a potential therapeutic strategy. We used hemin treatment in-vitro and a mouse autologous blood injection ICH model to study astrocytic TRPA1's effect on the phenotypic transformation of glial cells and the inflammatory response after ICH. The underlying mechanism and effect on neurological function were further investigated.

Materials and methods

Animals

To establish the ICH model, we used 97 adult male mice (age 8–10 weeks and weight 22–26 g), including 67 WT C57/BL6 mice (Laboratory Animal Center, Third Military Medical University, Chongqing, China, Ethical Batch No. AMUWEC2020761) and 30 TRPA1$^{-/-}$ mice (NM-KO-190446; Shanghai Model Organisms Center). Primary neurons and astrocytes were extracted from nine pregnant mice (E16-E18) and 21 mouse pups (P0-P2). After the sexual maturation of transgenic mice, their genotypes were identified by a mouse tail genotype–identification kit (Bimake, Houston, Texas, USA; Cat: B40015). The mice were kept in a room with constant temperature, 12 h cycle of day and night, and free access to food and water throughout the experimental period. All the experiments met the guidelines of ARRIVE and the National Institutes of Health Guide for the Care and Use of Laboratory Animals (NIH Publications No. 80-23, revised 2011). The experimental design of the whole study is shown in Fig. 1a.

Intracerebral hemorrhage model

Specific steps to establish the ICH model refer to previous literature [15]. In brief, we used a mixed gas of 2% isoflurane and air to anesthetize mice, fixed them on a stereotaxic apparatus, and maintained anesthesia. The mouse head was disinfected by skin preparation, and an incision of approximately 1 cm was longitudinally cut along the midpoint of the line between the two ears. The mouse bregma was used as the origin, and the coordinates (0.9 mm in front and 2.1 mm beside on the right) were located. A skull drill drilled a small hole. Fifteen microliters of autologous blood was collected from the tail of the mice, a microsyringe needle (Hamilton, Bonaduz, Switzerland; Cat: RN1702) was positioned at a depth of 3 mm, and 5 μl (1.5 μl/min) of blood was injected under the assistance of a microinjection pump (KD Scientific, Holliston, Massachusetts, USA). The needle was stopped for 1 min, and then, the microsyringe was repositioned at a depth of 3.3 mm. The remaining 10 μl (1.5 μl/min) of blood was injected. After the blood injection, the needle was stopped for 5 min and slowly withdrawn. ICH mice that died without symptoms or before the end of the experiment were excluded. We performed all the operations mentioned above for the sham group except for the blood injection. According to our previous study, we assessed behavioral and pathological changes in the acute phase of ICH in mice on days 1 and 3 [14].

Culture of primary neurons and primary astrocytes

The literature describes the extraction of primary neurons and astrocytes [16]. Briefly, cervical transection was performed to kill pregnant mice on pregnancy days 16–18, and the cortex of the fetus was quickly removed. Then, the cerebral pial tissue of the cortex was removed under a microscope. The brain tissue was disrupted and digested with 0.125% trypsin at 37 °C for 30 min. Medium containing serum was added to stop digestion, the supernatant was discarded by centrifugation at 800 rpm for 5 min, and a single-cell suspension was collected after resuspension and filtration. A cell counter counted the cells, and then, the cells were placed in a six-well plate precoated with 0.0125 mol/l poly-L-lysine (Thermo Scientific, Waltham, Massachusetts,

Fig. 1

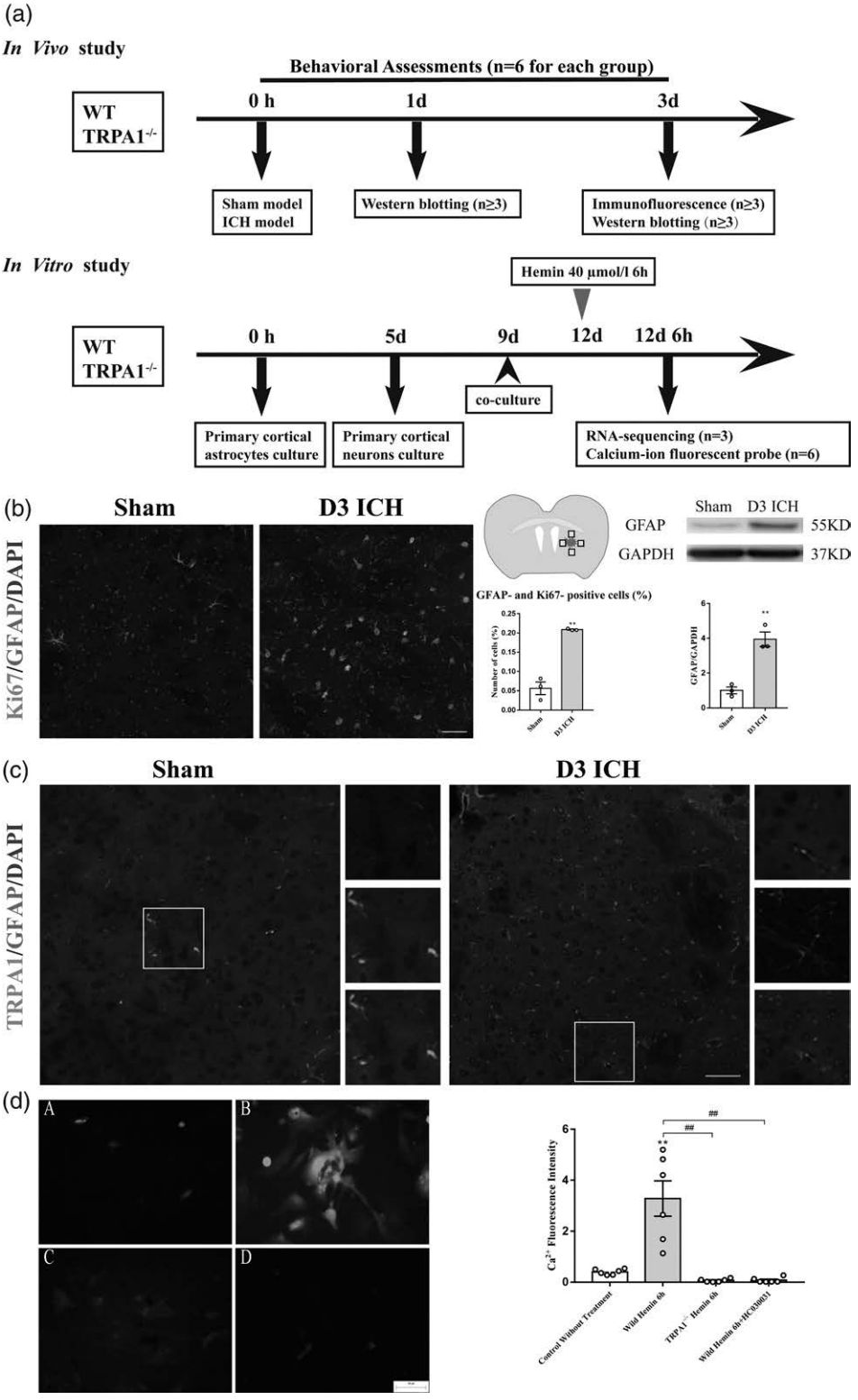

Hyperplasia of astrocytes around a hematoma and inhibition of calcium elevation by TRPA1 knockout after intracerebral hemorrhage (ICH). (a) Experimental outline of the in-vivo and in-vitro experiments. (b) Immunofluorescence of GFAP and Ki67 and western blot analysis of GFAP after ICH ($n = 3$). (c) Immunofluorescence of TRPA1 and GFAP after ICH. (d) Fluorescent images of Ca^{2+} levels in astrocytes stained with Fluo-4 AM dye and statistical histogram ($n = 6$). Unless otherwise specified, scale bars represent 50 μm ($^{**}P < 0.01$ vs. sham group, $^{\#\#}P < 0.01$). GFAP, glial fibrillary acidic protein; TRPA1, transient receptor potential ankyrin 1.

USA; Cat: A3890401) at 1×10^6 cells/ml. Dulbecco's modified eagle medium (DMEM)/F12 (Gibco, Grand Island, New York, USA; Cat: C11330500BT) supplemented with 10% fetal bovine serum (Gibco, Grand Island, New York, USA; Cat: 10091148) and 10% horse serum (Procell, Wuhan, China; Cat: 164215) was used as the medium, and the plate was placed in a 37 °C, 5% CO_2 incubator. After 4 h, the medium was replaced with serum-free neuron medium consisting of neurobasal medium (Gibco, Grand Island, New York, USA; Cat: 21103049) supplemented with 2% B27-supplement (Gibco, Grand Island, New York, USA; Cat: 17504044) and 1% Glutamax-I (Gibco, Grand Island, New York, USA; Cat: 35050061). After 5 days, the cell medium was replaced with fresh medium.

The cortex of mouse pups (P0–P2) was separated to remove the cerebral pial tissue under a microscope. The brain tissue was disrupted and digested with 0.25% trypsin at 37 °C for 7–8 min. Medium consisting of DMEM (Gibco, Grand Island, New York, USA; Cat: C11995500BT) supplemented with 10% fetal bovine serum and penicillin/streptomycin (Gibco, Grand Island, New York, USA; Cat: 15140122, 1 ml/100 ml) was added to terminate the digestion, and 100-µl DNA enzyme (10 mg/ml; Sigma-Aldrich, Saint Louis, Missouri, USA; Cat: DN25) was added. The supernatant was discarded by centrifugation at 1000 rpm for 10 min, and a single-cell suspension was collected after resuspension and filtration. The cells were placed in a T-25 culture flask. Fresh medium was replaced the next day. After being cultured in-vitro for 7–8 days, the astrocytes were shaken in a shaker for 24 h at 37 °C and 200 rpm speed. After digestion, centrifugation, resuspension, and counting, the cells were placed in 12-well plates (2.5×10^5 cells/ml) for calcium-ion fluorescent probe experiments. To simulate the ICH model in-vitro, hemin (Sigma-Aldrich, Saint Louis, Missouri, USA; Cat: 51280; 40 µmol/l) was added to the medium to treat the astrocytes for 6 h, according to previous research [17].

Astrocyte-neuron coculture

Primary astrocytes were extracted according to the above method, and the astrocytes were first seeded in a T-25 culture flask. On the fifth day, primary neurons were extracted according to the above method and seeded in six-well plates (2×10^6 cells/ml). On the seventh day, the astrocytes were purified in a T-25 culture flask according to the above protocol, and then, the purified astrocytes were seeded in a 0.4-µm Transwell (Merck Millipore, Darmstadt, Germany; Cat: MCHT06H48; 0.5×10^6 cells/ml). The Transwells were placed above six-well plates on the ninth day for astrocyte-neuron coculture. Then, 2.6-ml neuron medium was added to the six-well plate, and 1.5-ml neuron medium was added to the upper Transwells. The cocultured cells were used for an RNA-seq experiment on the 12th day. The culture times of neuron, astrocyte, and astrocyte-neuron cocultures were based on a previous study [10]. To simulate the ICH model in-vitro, hemin (40 µmol/l) was added to the medium to treat the astrocyte-neuron coculture for 6 h.

Experimental groups and sample sizes

Mice were randomly separated into groups (Sham, WT ICH, and $TRPA1^{-/-}$ ICH) using a computer-generated list. The astrocyte groupings were as follows: a control without treatment group, a wild-type hemin 6 h group, a $TRPA1^{-/-}$ hemin 6 h group, and a wild-type hemin 6 h + HC030031 group (80 µmol/l); $n = 6$ for each group. The TRPA1 antagonist HC-030031 was obtained from Sigma-Aldrich (Saint Louis, Missouri, USA; Cat: H4415) [13]. The astrocyte-neuron cocultures were divided into three groups: neurons + astrocytes control group, neurons + astrocytes+hemin 6 h group, and neurons + $TRPA1^{-/-}$ astrocytes+hemin 6 h group; $n = 3$ for each group.

Immunofluorescence

After the mice were perfused with normal saline and 4% paraformaldehyde solution, the brains of the mice were collected, fixed in 4% paraformaldehyde solution for 1 day, and then placed in 30% sucrose solution prepared with 0.01 mol/l PBS for dehydration for 2 days. The brain slices were serially sliced (25 µm) with a cryostat microtome (CM1860UV, Leica, Wetzlar, Germany). The brain slices were blocked (0.3% Triton for 30 min and 5% BSA for 1 h) and incubated with the following primary antibodies: rabbit anti-Ki67 (1:200; Abcam, Cambridge, UK; Cat: ab15580), mouse anti-TRPA1 (1:200; Santa Cruz, Dallas, Texas, USA; Cat: sc-376495), rat anti-glial fibrillary acidic protein (GFAP) (1:200; Invitrogen, Carlsbad, California, USA; Cat: VB298933), mouse anti-ionized calcium binding adapter molecule 1 (Iba1) (1:500; Wako, Kanagawa, Japan; Cat: 019-19741), mouse anti-S100 calcium binding protein A10 (S100A10) (1:400; Cell Signaling Technology, Danvers, Massachusetts, USA; Cat: 5529S), and mouse anti-arginase-1 (ARG-1) (1:500; BD Biosciences, Franklin Lake, New Jersey, USA; Cat: 610709). After brain slices were washed, they were incubated with Alexa Fluor 488- or Alexa Fluor 555-conjugated secondary antibody (1:1000; Invitrogen, Carlsbad, California, USA) and costained with 4'-6-diamidino-2-phenylindole (DAPI). A confocal microscope (Zeiss, LSM880, Oberkochen, Germany) was used to photograph the tissues surrounding the hematoma. FIJI software (Version 2.0, National Institutes of Health, Bethesda, Maryland, USA) and the Sholl analysis plugin performed the morphological analysis of 40× magnification images. The circularity index (CI) and the Shoenen ramification index (RI) were calculated [18].

Western blotting

The tissue around the hematoma was homogenized, and the protein was extracted with lysis buffer containing protease and phosphatase inhibitors (Thermo Fisher, Waltham, Massachusetts, USA; Cat: 78510). The protein concentration was determined with a Beyotime protein concentration detection kit (Shanghai, China). A 4–12.5% SDS gradient polyacrylamide gel (30 µg of protein per lane) was used for a standard blotting procedure. After the process, the polyvinylidene fluoride (PVDF) membranes containing proteins

were incubated with the following primary antibodies at 4 °C overnight: rat anti-GFAP (1:1000; Invitrogen, Carlsbad, California, USA; Cat: VB298933), rabbit anti-IL-6 (1:1000; Abcam, Cambridge, UK; Cat: ab179570), mouse anti-TNF-α (1:500; Santa Cruz, Dallas, Texas, USA; Cat: sc-52746), rabbit anti-Iba1 (1:1000; Cell Signaling Technology, Danvers, Massachusetts, USA; Cat: 17198), rabbit anti-IL-1β (1:1000; GeneTex, San Antonio, Texas, USA; Cat: GTX74034), rabbit anti-extracellular regulated protein kinase (ERK) (1:1000, Cambridge, UK; Abcam; Cat: ab17942), rabbit anti-p-ERK (1:2000, Cambridge, UK; Abcam; Cat: ab201015), rabbit anti-inhibitor kappa B kinaseβ (IKKβ) (1:1000; Cell Signaling Technology, Danvers, Massachusetts, USA; Cat: 8943), rabbit anti-p-IKKβ (1:1000; Cell Signaling Technology, Danvers, Massachusetts, USA; Cat: 2697), mouse anti-ARG-1 (1:500; BD Biosciences, Franklin Lake, New Jersey, USA; Cat: 610709), mouse anti-S100A10 (1:1000; Cell Signaling Technology, Danvers, Massachusetts, USA; Cat: 5529S), mouse anti-GAPDH (1:8000, ZEN BIO, Chengdu, China; Cat: 200306-7E4), mouse anti-β-actin (1:2000; Boster, Wuhan, China; Cat: BM0627), and rabbit antitubulin (diluted 1:1000, Proteintech, Wuhan, China, Cat:10094-1-AP). After thorough washing, the membranes were incubated with the corresponding horseradish peroxidase (HRP)–conjugated IgG (1:10000; Proteintech, Wuhan, China) at room temperature for 2 h. The protein bands were visualized using ECL kits (Thermo Scientific, Waltham, Massachusetts, USA) and detected with a bioimaging system (ChemiDoc XRS+; Bio-Rad, Hercules, California, USA). The blot bands were analyzed using the Image Lab software (Image Lab 3.0; Bio-Rad, Hercules, California, USA).

Calcium-ion fluorescent probe

According to the instructions, Fluo-4 AM (Beyotime, Shanghai, China; Cat: S1060) was used to detect the changes in calcium ions in astrocytes. Briefly, the calcium ion probe (1:1000) was added to a fresh medium to configure the working fluid. Using the working fluid to replace the medium, the cells were incubated at 37 °C for 45 min, and then, the working fluid was replaced with PBS. The fluorescence intensity of the calcium ion probe was detected by fluorescence microscopy.

RNA-sequencing

TRIzol (Thermo Scientific, Waltham, Massachusetts, USA; Cat: 15596018) was used to isolate and purify RNA from the three groups according to the operation scheme provided by the manufacturer, and then, the samples were sent to LC Science for total RNA sequencing. Cutadapt and in-house Perl scripts were used to remove the reads that contained adaptor contamination, low-quality bases, and undetermined bases. Then, sequence quality was verified using FastQC (http://www.bioinformatics.babraham.ac.uk/projects/fastqc/). We aligned reads of all samples to the *Mus musculus* reference genome using HISAT2 (https://daehwankim-lab.github.io/hisat2/, version: hisat2-2.0.4) package, which initially removed a portion of the reads based on quality information accompanying each read and then mapped the reads to the reference genome. The mapped reads of each sample were assembled using StringTie (http://ccb.jhu.edu/software/stringtie/, version: stringtie-1.3.4d) with default parameters. Then, all transcriptomes from all samples were merged to reconstruct a comprehensive transcriptome using the gffcompare software (http://ccb.jhu.edu/software/stringtie/gffcompare.shtml, version: gffcompare-0.9.8). After the final transcriptome was generated, StringTie and Ballgown (http://www.bioconductor.org/packages/release/bioc/html/ballgown.html) were used to estimate the expression levels of all transcripts and determine the expression abundance of mRNAs by calculating the fragment per kilobase of transcript per million mapped reads value. Gene differential expression analysis was performed by DESeq2 software (Michael Love, Simon Anders, Wolfgang Huber; USA) between two groups (and by edgeR between two samples). Genes with a false discovery rate below 0.05 and absolute fold change at least 2 were considered differentially expressed genes [19].

Behavioral assessments

All behavioral assessments were conducted at the corresponding time points and recorded by a digital video camera. The mice were weighed before the behavioral test. The results were analyzed in a blinded manner.

Basso mouse scale

The open-field locomotor scoring system ranges from 0 points (no ankle movement) to 9 points (mainly coordinated, paws parallel at initial contact and lift off, frequent or consistent plantar stepping, normal trunk stability, and tail always up) [14].

Beam balance test

The mouse was allowed to cross a round wooden beam 70 cm in length, 1.5 cm in diameter, and elevated 30 cm from the ground for 1 min. The walking distance and gait determined the score (0–4). The average score of three consecutive trials was calculated [14].

Mouse forelimb grip strength

The mouse forelimb grip strength was measured with a grip strength meter (1027SM Columbus Instruments, Columbus, Ohio, USA).

Statistical analysis

All data were analyzed using the SPSS 22.0 software (IBM, Armonk, New York, USA). The data are shown as the mean ± SEM. The Shapiro-Wilk normality test was used to assess the distribution of the data. A two-tailed Student's *t*-test was used to compare the two groups. One-way analysis of variance (ANOVA) followed by Tukey's post hoc test was used to analyze the difference in calcium fluorescent probe intensity, fluorescence intensity,

CI, Shoenen RI, and protein expression between different groups. The behavioral and activity scores were analyzed using two-way repeated-measures ANOVA. If the data were not normally distributed, analysis was performed using nonparametric statistics. $P < 0.05$ was considered statistically significant.

Results

Hyperplasia of astrocytes around the hematoma and knockout of TRPA1 attenuated the elevation of calcium in astrocytes following intracerebral hemorrhage

Astrocytes, in response to various forms of central nervous system injury and diseases, occur in a series of gene expression, cell structure, and function changes called astrocyte hyperplasia. In this study, GFAP and Ki67 were used to evaluate the proliferation and hypertrophy of astrocytes around the hematoma in mice with ICH. The results showed that compared with the sham group, the proportion of GFAP/Ki67-positive cells was increased ($P = 0.0007$, $n = 3$), and the expression of GFAP protein around the hematoma in ICH mice was enhanced ($P = 0.0031$, $n = 3$) (Fig. 1b). Next, we explored the expression of TRPA1 on astrocytes. TRPA1 and GFAP immunofluorescence colabelling showed that TRPA1 was expressed on astrocytes (Fig. 1c).

We cultured astrocytes and treated them with hemin to simulate ICH in-vitro. We then examined the effect of TRPA1 on calcium activity in astrocytes after ICH. The results showed that astrocytes treated with 40 μmol/l hemin for 6 h presented a higher fluorescence intensity of the calcium ion probe than the control group ($P < 0.0001$, $n = 6$). However, with simultaneous application of the TRPA1 blocker HC030031 and hemin to astrocytes ($P < 0.0001$, $n = 6$) or TRPA1$^{-/-}$ astrocytes treated with 40-μmol/l hemin ($P < 0.0001$, $n = 6$) for 6 h, the fluorescence intensity of the calcium ion probe was significantly decreased compared with that of astrocytes treated with 40-μmol/l hemin for 6 h ($F_{(3, 20)} = 19.97$, $P < 0.0001$) (Fig. 1d). This result indicated that blocking or knocking out TRPA1 could reduce the calcium ion flow into astrocytes after hemin treatment.

Conversion of TRPA1$^{-/-}$ astrocytes to A2 astrocytes after intracerebral hemorrhage

The study showed that astrocyte calcium ion activity could affect the astrocyte phenotype, so we cocultured astrocytes and neurons and performed transcriptome sequencing of astrocytes [20]. After resequencing and analyzing a single sample, the Pearson correlation between samples (hemin 6 h group vs. control group; TRPA1$^{-/-}$ hemin 6 h group vs. hemin 6 h group) showed three different groups (Fig. 2a). In general, our analysis found 1335 differentially expressed genes (424 upregulated and 911 downregulated) after hemin treatment of astrocytes. After hemin treatment of TRPA1$^{-/-}$ astrocytes, compared with hemin treatment of astrocytes, there were 615 differentially expressed genes (380 upregulated and 235 downregulated). The top 30 differentially expressed genes are shown in Fig. 2b. The results revealed that canonical markers of reactive astrogliosis and panreactive transcripts, such as Cxcl10 and Cd44, were upregulated after hemin treatment. We also analyzed the phenotype of astrocytes after hemin treatment. The results showed that some specific transcripts of A1 and A2 were upregulated after hemin treatment (Fig. 2c). However, after hemin 6 h treatment of TRPA1$^{-/-}$ astrocytes, compared with the astrocytes treated with hemin 6 h, the A2-specific transcript Tm4sf1 was significantly upregulated (Fig. 2d). Next, we detected changes in S100A10, which is a marker of A2 astrocytes, after ICH. The results indicated that the fluorescence intensity of S100A10 around the hematoma in TRPA1$^{-/-}$ ICH mice was enhanced compared with that in wild-type ICH mice ($P < 0.0001$, $n = 5$) ($F_{(2, 12)} = 55.88$, $P < 0.0001$), and the expression of S100A10 was increased ($P < 0.0001$, $n = 3$) ($F_{(2, 6)} = 225.9$, $P < 0.0001$) (Fig. 2e).

TRPA1 knockout in astrocytes alleviated the inflammatory response around the hematoma by inhibiting the MAPK/NF-κB signaling pathway

Various inflammatory factors increase after stroke, such as TNF-α, IL-1β, and IL-6. We detected inflammation around the hematoma in TRPA1$^{-/-}$ ICH mice, and the results showed that the expression levels of IL-1β ($P < 0.0001$, $n = 3$) and IL-6 ($P < 0.0001$, $n = 3$) in wild-type mice were increased on D1 ICH. However, in TRPA1$^{-/-}$ ICH mice, compared with that in wild-type ICH mice, the expression levels of IL-1β ($P = 0.0058$, $n = 3$) ($F_{(4, 10)} = 24.62$, $P < 0.0001$) and IL-6 ($P < 0.0001$, $n = 3$) ($F_{(4, 10)} = 45.56$, $P < 0.0001$) were decreased on D1, indicating that the inflammatory response around the hematoma in the acute stage was alleviated (Fig. 3a and b). Interestingly, our results showed that the expression of TNF-α in wild-type mice was increased on D1 ICH. In contrast, the expression of TNF-α in TRPA1$^{-/-}$ ICH mice was increased significantly compared with that in wild-type ICH mice ($P < 0.0001$, $n = 5$) ($F_{(4, 20)} = 52.07$, $P < 0.0001$) (Fig. 3c). According to previous studies, astrocytes have a close relationship with microglia in nervous system inflammation. Microglia can secrete TNF-α to promote reactive astrocyte proliferation [6,21]. It has been reported that TRPA1 promotes cisplatin-induced nephrotoxicity through inflammation mediated by the mitogen-activated protein kinase (MAPK)/nuclear factor kappa-B (NF-κB) signaling pathway [22]. Our results showed that the expression of p-ERK ($P < 0.0001$, $n = 4$) ($F_{(4, 15)} = 29.4$, $P < 0.0001$) and the ratio of p-ERK/ERK ($P < 0.0001$, $n = 4$) ($F_{(4, 15)} = 16.1$, $P < 0.0001$) in TRPA1$^{-/-}$ mice were decreased compared to those in WT mice on D1 ICH. p-IKKβ expression was decreased in TRPA1$^{-/-}$ mice compared with WT mice on D3 ICH ($P = 0.0022$, $n = 3$) ($F_{(4, 10)} = 27.56$, $P < 0.0001$), and the ratio of p-IKKβ/IKKβ was decreased in TRPA1$^{-/-}$ mice compared with WT mice on D1 ICH ($P = 0.0046$, $n = 3$) and D3 ICH ($P = 0.0065$, $n = 3$) ($F_{(4, 10)} = 37.02$, $P < 0.0001$) (Fig. 3d and e).

Fig. 2

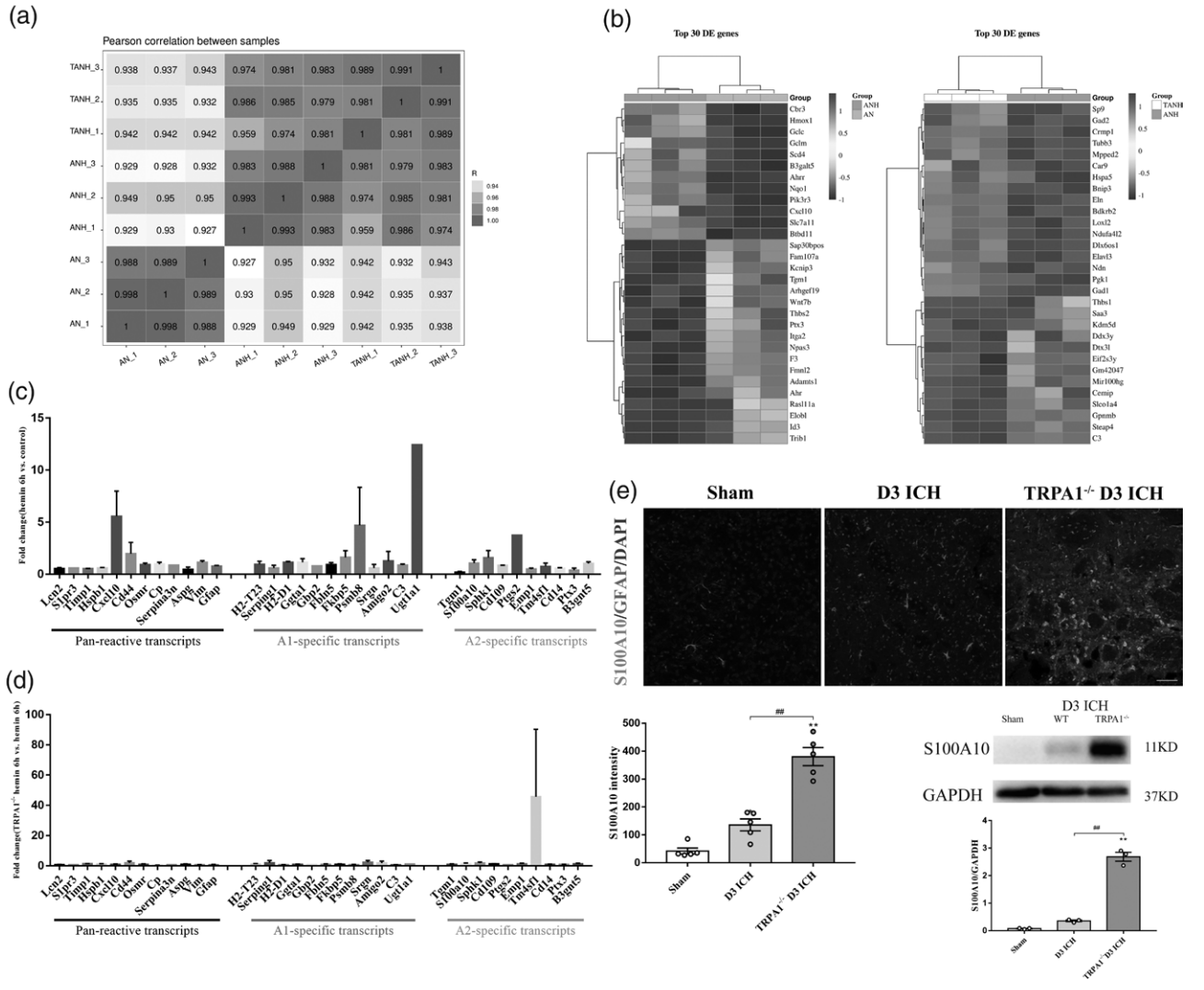

Conversion of TRPA1$^{-/-}$ astrocytes to A2 astrocytes after ICH. (a) Pearson correlation between samples (each sample representing astrocytes from one astrocyte-neuron coculture) of astrocyte mRNA from astrocyte-neuron coculture after hemin treatment (ANH, TANH) and control (AN) ($n = 3$). (b) The top 30 differentially expressed (DE) genes after hemin treatment compared with the control and the top 30 DE genes after TRPA1$^{-/-}$ astrocyte hemin treatment compared to astrocyte hemin treatment. (c) Bar graphs indicate the fold change in the expression of panreactive transcripts and A1- and A2-specific transcripts after hemin treatment of astrocytes. (d) Bar graphs reveal a predominance of A2-specific transcripts after hemin treatment of TRPA1$^{-/-}$ astrocytes. (e) Immunofluorescence for GFAP and S100A10 on D3 ICH. The fluorescence intensity of S100A10 was analyzed. Western blot analysis of S100A10 protein levels in brain tissue around the hematoma in the sham, D3 ICH, and TRPA1$^{-/-}$ D3 ICH groups ($n \geq 3$) ($^{*}P < 0.05$ vs. sham group, $^{**}P < 0.01$ vs. sham group, $^{\#\#}P < 0.01$). GFAP, glial fibrillary acidic protein; ICH, intracerebral hemorrhage; S100A10, S100 calcium binding protein A10; TRPA1, transient receptor potential ankyrin 1.

TRPA1 knockout in astrocytes increased the proliferation of astrocytes and microglia with phagocytic capacity

We detected GFAP and Ki67 around the hematoma in TRPA1$^{-/-}$ ICH mice. Compared with those in wild-type ICH mice, the proportion of GFAP/Ki67-positive cells ($P = 0.0003$, $n = 5$) ($F_{(2, 12)} = 44.17$, $P < 0.0001$) and the expression of GFAP in TRPA1$^{-/-}$ mice were increased after ICH ($P = 0.0082$, $n = 3$) ($F_{(2, 6)} = 61.57$, $P = 0.0001$) (Fig. 4a). Next, we observed changes in microglia around the hematoma. The results showed that microglial proliferated obviously around hematoma. The expression of Iba1, a microglial marker, was further increased around the hematoma in TRPA1$^{-/-}$ ICH mice compared with that in wild-type ICH mice ($P = 0.0319$, $n = 9$) ($F_{(2, 24)} = 21.99$, $P < 0.0001$). The proportion of Iba1/Ki67-positive cells was higher in TRPA1$^{-/-}$ ICH mice ($P = 0.0099$, $n = 4$) ($F_{(2, 9)} = 39.08$, $P < 0.0001$) (Fig. 4b). ARG-1 is a conventional marker of M2 microglia, which can reduce inflammation, improve neuronal and white matter damage, and promote the recovery of neurological function after ICH [21,23]. The results

Fig. 3

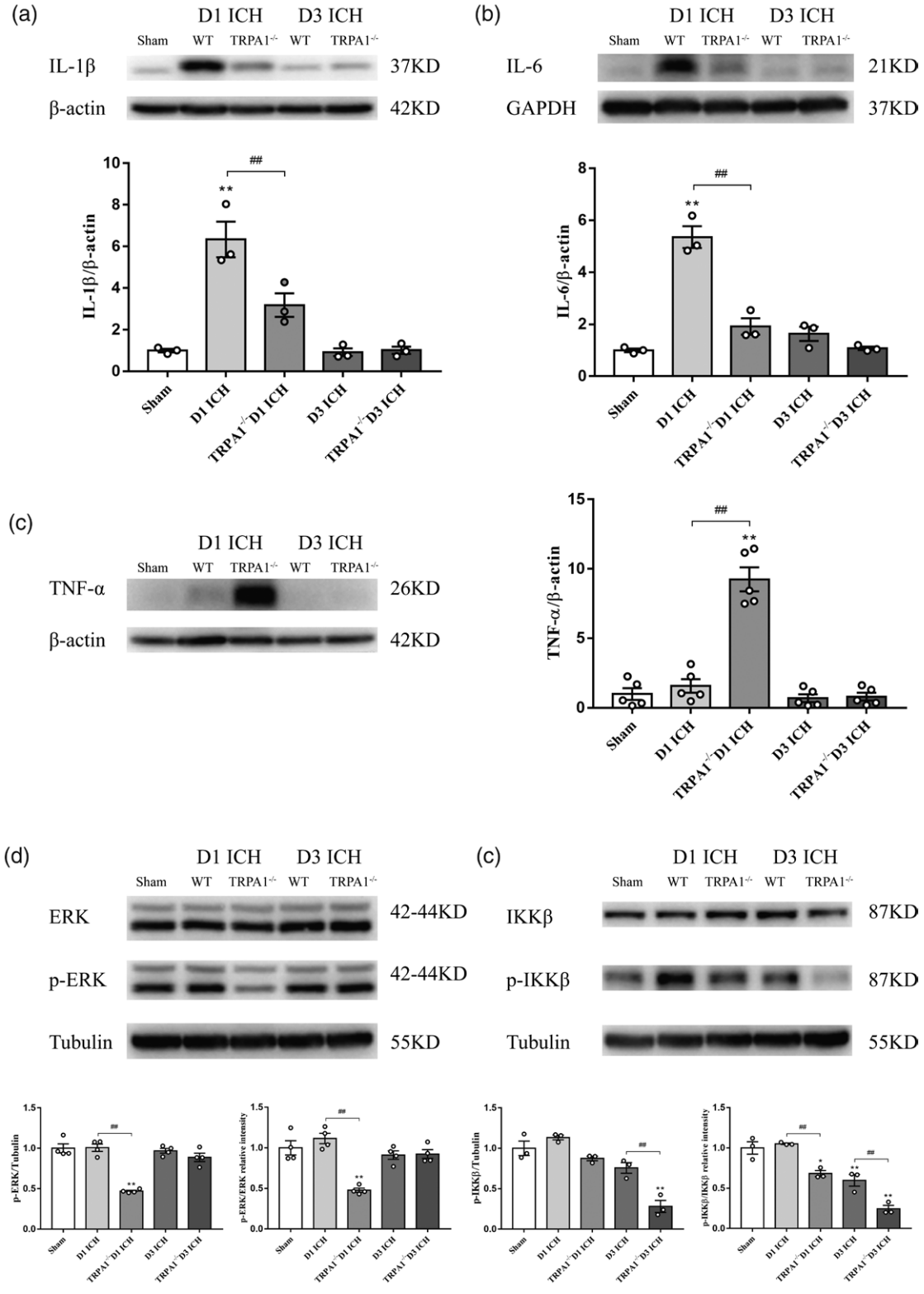

Alleviation of inflammation around the hematoma in TRPA1$^{-/-}$ ICH mice mediated by the MAPK/NF-κB signaling pathway. (a–c) Western blot analysis and quantification of IL-1β, IL-6, and TNF-α protein levels in brain tissue around the hematoma in different groups ($n \geq 3$). (d and e) The expression of p-ERK and p-IKKβ and the ratio of p-ERK/ERK and p-IKKβ/IKKβ in brain tissue around the hematoma in different groups ($n \geq 3$) (**$P < 0.01$ vs. sham group, $^{\#}P < 0.05$, $^{\#\#}P < 0.01$). ERK, extracellular regulated protein kinase; ICH, intracerebral hemorrhage; IKKβ, inhibitor kappa B kinaseβ; IL, interleukin; MAPK/NF-κB; TNF-α, tumor necrosis factor-α; TRPA1, transient receptor potential ankyrin 1.

Fig. 4

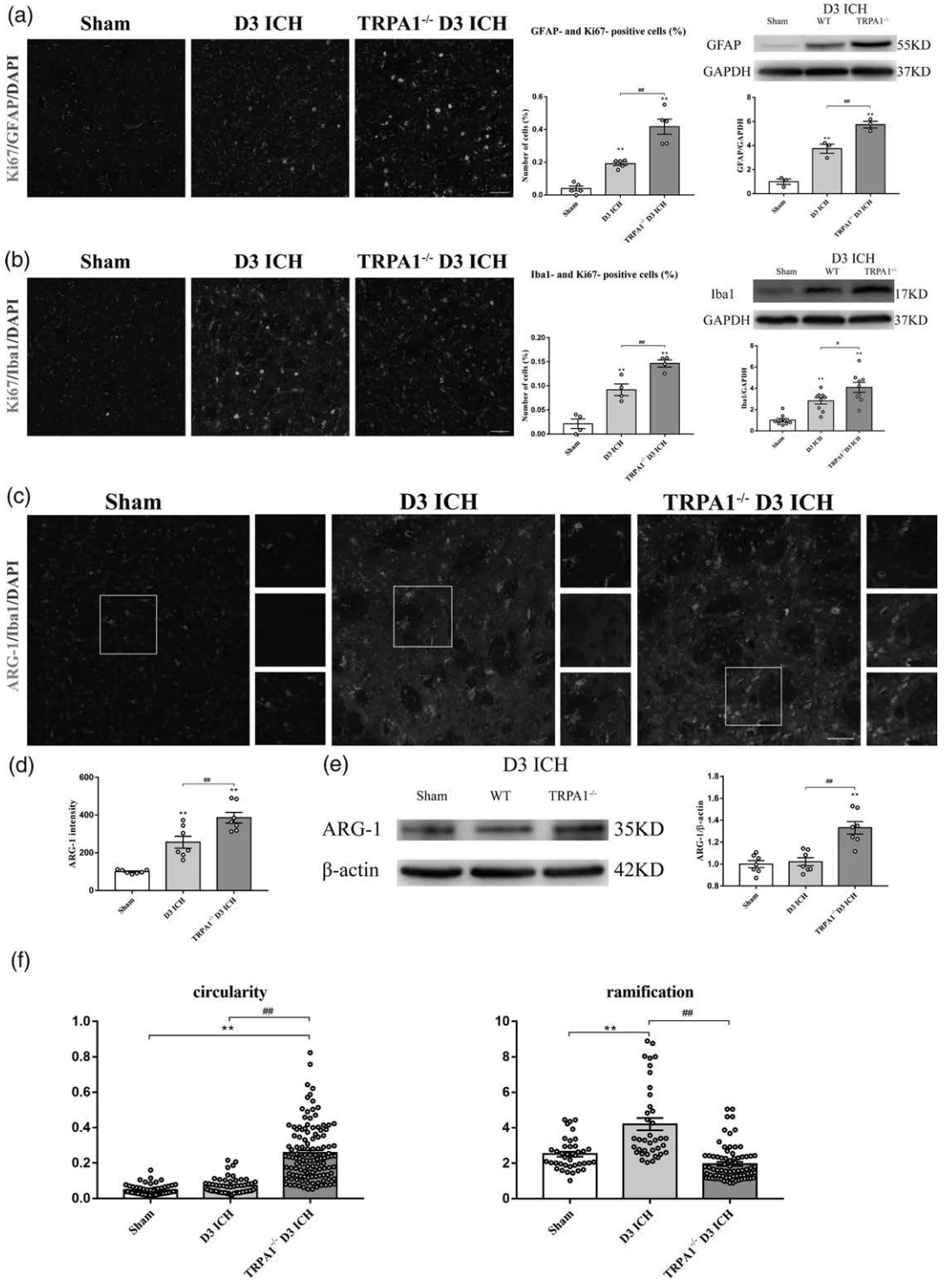

The proliferation of astrocytes and microglia around the hematoma in TRPA1$^{-/-}$ ICH mice and the proliferated microglia transformed into the 'ameboid' microglia on D3 ICH. (a) Immunofluorescence of GFAP and Ki67 and western blot analysis of GFAP around the hematoma in the sham, D3 ICH, and TRPA1$^{-/-}$ D3 ICH groups ($n \geq 3$). (b) Immunofluorescence of Iba1 and Ki67 and western blot analysis of Iba1 around the hematoma in the sham, D3 ICH, and TRPA1$^{-/-}$ D3 ICH groups ($n \geq 3$). (c and d) Immunofluorescence for Iba1 and ARG-1 on D3 ICH. The fluorescence intensity of ARG-1 was analyzed ($n = 7$). (e) Western blot analysis and the quantification of ARG-1 protein levels in brain tissue around the hematoma in the sham, D3 ICH, and TRPA1$^{-/-}$ D3 ICH groups ($n = 7$). (f) The circularity index (left) and Shoenen ramification index (right) of microglia around the hematoma. Fifty-five to 121 cells per group of $n = 5$ mice. Unless otherwise specified, scale bars represent 50 μm ($^{**}P < 0.01$ vs. sham group, $^{\#}P < 0.05$, $^{\#\#}P < 0.01$). ARG-1, arginase-1; GFAP, glial fibrillary acidic protein; ICH, intracerebral hemorrhage; TRPA1, transient receptor potential ankyrin 1.

showed that compared with that in wild-type ICH mice, the fluorescence intensity of ARG-1 around the hematoma in TRPA1$^{-/-}$ ICH mice was enhanced ($P = 0.0038$, $n = 7$) ($F_{(2, 18)} = 34.54$, $P < 0.0001$), and the expression of ARG-1 was increased ($P = 0.0002$, $n = 7$) ($F_{(2, 18)} = 18.48$, $P < 0.0001$) (Fig. 4c–e). Compared with wild-type ICH mice, the CI of microglia of TRPA1$^{-/-}$ ICH mice was increased ($P < 0.0001$, $n = 5$) ($F_{(2, 233)} = 88.81$, $P < 0.0001$), and the Shoenen RI of microglia of TRPA1$^{-/-}$ ICH mice was decreased ($P < 0.0001$, $n = 5$) ($F_{(2, 150)} = 35.95$, $P < 0.0001$) (Fig. 4f). These results indicated that the morphology of the microglia changed from ramified to rounded. These 'ameboid' microglia were reported to have a phagocytic capacity, which could improve hematoma absorption [24].

TRPA1$^{-/-}$ mice displayed better behavioral performance than wild-type mice after intracerebral hemorrhage

We used three behavioral tests to assess the neurological function of mice. Compared with sham group mice, wild-type ICH mice showed a lower score on the Basso mouse scale on D1($P < 0.0001$, $n = 6$) and D3 ($P = 0.0016$, $n = 6$). TRPA1$^{-/-}$ ICH mice presented a higher score than wild-type ICH mice on D3 ($P = 0.0093$, $n = 6$) (main effect of group: $F_{(2,15)} = 11.11$, $P = 0.0011$; two-way interaction: $F_{(4,30)} = 6.125$, $P = 0.001$) (Fig. 5a). The beam balance test scores of wild-type ICH mice ($P < 0.0001$, $n = 6$) and TRPA1$^{-/-}$ ICH mice ($P = 0.0038$, $n = 6$) were lower than those of sham group mice on D1, and the beam balance test scores of TRPA1$^{-/-}$ ICH mice were higher than those of wild-type ICH mice on D1 ($P = 0.0065$, $n = 6$) and D3 ($P = 0.0109$, $n = 6$) (main effect of group: $F_{(2,15)} = 14.06$, $P = 0.0004$; two-way interaction: $F_{(4,30)} = 6.345$, $P = 0.0008$) (Fig. 5b). The forelimb grip strength of wild-type ICH mice was lower than that of sham mice on D1 ($P < 0.0001$, $n = 6$) and D3 ($P < 0.0001$, $n = 6$), and TRPA1$^{-/-}$ ICH mice displayed better forelimb grip strength than wild-type ICH mice on D3 ($P < 0.0001$, $n = 6$) (main effect of group: $F_{(2,15)} = 33.53$, $P < 0.0001$; two-way interaction: $F_{(4,30)} = 20.51$, $P < 0.0001$) (Fig. 5c).

Discussion

After ICH, various endogenous molecules are released, which aggravate the oxidative stress response and interrupt cellular signaling pathways through neuroinflammation, resulting in cytotoxicity and excitotoxicity, and ultimately leading to secondary brain injury after ICH. Hematoma metabolites activate astrocytes, and astrocytes proliferate and accumulate in the surrounding areas of the hematoma, which further produce and release cytokines and chemokines to aggravate the inflammatory response. These changes will lead to the death of neurons and other glial cells in the acute phase of ICH, damage axon fiber bundles, and lead to motor dysfunction in patients. Therefore, exploring the mechanism of the inflammatory response is crucial after ICH.

The inflammatory response after ICH mainly involves astrocytes, microglia, and their interactions. Recent studies have found that astrocytes can be divided into groups that mediate proinflammatory, toxic effects of the A1 phenotype, and neuroprotection effects of the A2 phenotype. The diverse phenotypical and functional heterogeneity of microglia is observed in the brain relating to the development, homeostasis, aging, and response to injury [4,5]. Moreover, astrocytes and microglia can secrete factors to affect their phenotypes, influencing the inflammatory response. We observed the proliferation of astrocytes around the hematoma in ICH. Furthermore, the changes in calcium ions in astrocytes treated with hemin proved that TRPA1 played an essential role in the calcium influx of astrocytes after ICH. Astrocytic TPRA1 knockout was found to affect the natural process of glial phenotype transformation after ICH. After RNA sequencing of astrocyte-neuron cocultures, we found that some specific transcripts of the A1 and A2 phenotypes were increased after hemin treatment. The specific transcript of the A2 phenotype was further increased after hemin treatment of TRPA1$^{-/-}$ astrocytes, which indicated that the proliferation of astrocytes converted to the protective A2 phenotype. The results of immunofluorescence and western blotting of S100A10 further confirmed this phenomenon.

Fig. 5

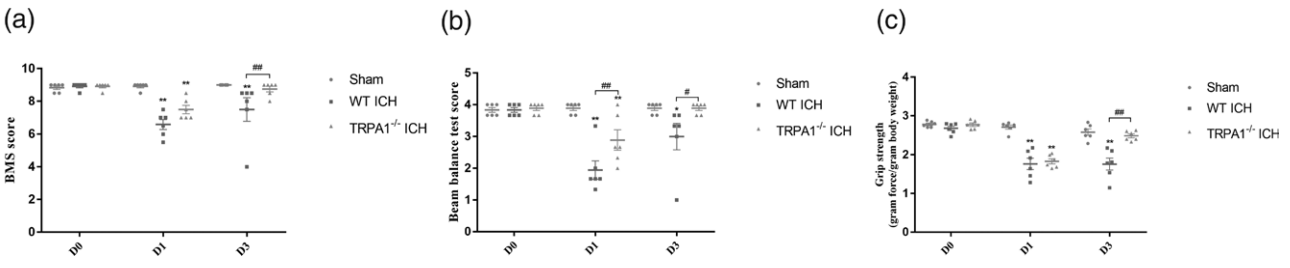

TRPA1$^{-/-}$ mice displayed better neurological function than wild-type mice after ICH. (a) BMS scores ($n = 6$). (b) Beam balance test scores ($n = 6$). (c) Forelimb grip strength ($n = 6$) (*$P < 0.05$ vs. sham group, **$P < 0.01$ vs. sham group, $^{\#}P < 0.05$, $^{\#\#}P < 0.01$). BMS, Basso mouse scale; ICH, intracerebral hemorrhage; TRPA1, transient receptor potential ankyrin 1.

Furthermore, we found that microglia around the hematoma proliferated and transformed into 'ameboid' microglia in TRPA1$^{-/-}$ ICH mice. The morphological change of microglia from ramified to rounded was observed around the hematoma in TRPA1$^{-/-}$ ICH mice. The proliferation of A2 astrocytes and 'ameboid' microglia ameliorated the neuroinflammation after ICH. According to previous research, the MAPK and NF-κB signaling pathways can trigger the production and release of numerous proinflammatory cytokines, such as IL-1β, IL-6, TNF-α, and interferon-γ, and the TRPA1 antagonist HC-030031 can inhibit the MAPK/NF-κB signaling pathway [18]. Our data showed that the inflammatory response of TRPA1$^{-/-}$ ICH mice was reduced by inhibiting the MAPK/NF-κB signaling pathway, and neurological function was improved.

There are few studies on the astrocyte phenotype after ICH. Our study first found that TRPA1 on astrocytes could affect the phenotypic conversion of astrocytes and microglia after ICH. However, the current research also has some limitations. Based on relevant studies, we chose S100A10 as a marker of A2 astrocytes, but it cannot include all A2 astrocytes [25]. We did not detect changes in markers of A1 astrocytes. We need to rely on the differentially expressed genes we found to explore the mechanism of glial phenotype transformation. In addition, we observed an apparent proliferation of astrocytes and microglia in TRPA1$^{-/-}$ mice after ICH, but the underlying mechanism was not clear. Furthermore, we did not detect neuronal survival or fiber bundle structure and did not perform further assessments of neuroelectrophysiological function in this study. The role of astrocytic TRPA1 was only assessed in the acute phase of ICH, and there was no evaluation of its function in the long term.

This study mainly explored the role of astrocytic TRPA1 in the inflammatory response after ICH. ICH is accompanied by severe neuronal death and white matter fiber tract injury. Mitochondrial dysfunction also exists around the hematoma [2]. There is a close relationship between astrocytes and neurons, but the role of astrocytes in neuronal injury after ICH is still unclear. In ischemic stroke, the astrocyte-mediated inflammatory response aggravates the ischemic injury, and astrocytes can also exert a neuroprotective effect by reducing excitotoxicity and secreting neurotrophic factors. Astrocyte swelling can mediate excitatory toxic effects and lead to neuronal death after ischemic stroke [26]. Similarly, astrocytes may have beneficial and harmful effects on neurons after ICH. How to amplify the beneficial effect of astrocytes on neurons is of great significance. Our previous study showed that applying TRPA1 blockers in mice with ICH could reduce the damage to the white matter fiber bundle [14]. Combined with our current research results and the above problems, we aimed to verify the role of astrocytic TRPA1 in the transformation of the glial phenotype after ICH by conditional knockout of TRPA1 in astrocytes in mice and explore the effects of astrocytic TRPA1 on the neuronal cell body, white matter fiber bundles, and neuronal mitochondrial function after ICH and the related mechanisms.

Conclusion

In summary, our experimental results showed that TRPA1 on astrocytes had a particular effect on the transformation of astrocytes to the A2 phenotype and microglia to 'ameboid' microglia after ICH. Moreover, TRPA1$^{-/-}$ mice showed a reduced inflammatory response after ICH.

Acknowledgements

We sincerely appreciate LC-Bio Technology Co. Ltd. (Hangzhou, China) for their assistance with the RNA-seq analysis.

This study was supported by the National Natural Science Foundation of China (No. 82030036, No. 82202298, and No. 82001263) and the Chongqing Graduate Student Research Innovation Project (No. CYB20195).

H.F. and W.N.L designed the thought and conceived the whole article. M.X. and Y.J.C. wrote the article's first draft, analyzed the results, and cooperated to construct the results shown in the figures. M.X., Y.J.C., B.K.C., and X.F.R. performed the relevant experiments, including cell culture and ICH model. J.W. and J.L. helped with the animal behavior tests. X.Q.T., W.X.C., and R.H. analyzed and processed the data. All authors reviewed the results and approved the final version of the manuscript.

Conflicts of interest

There are no conflicts of interest.

References

1 Hostettler IC, Seiffge DJ, Werring DJ. Intracerebral hemorrhage: an update on diagnosis and treatment. *Expert Rev Neurother* 2019; **19**:679–694.
2 Fu X, Zhou G, Zhuang J, Xu C, Zhou H, Peng Y, *et al*. White matter injury after intracerebral hemorrhage. *Front Neurol* 2021; **12**:562090.
3 Hanley DF, Thompson RE, Rosenblum M, Yenokyan G, Lane K, McBee N, *et al*. Efficacy and safety of minimally invasive surgery with thrombolysis in intracerebral haemorrhage evacuation (MISTIE III): a randomised, controlled, open-label, blinded endpoint phase 3 trial. *Lancet* 2019; **393**:1021–1032.
4 Lan X, Han X, Li Q, Yang QW, Wang J. Modulators of microglial activation and polarization after intracerebral haemorrhage. *Nat Rev Neurol* 2017; **13**:420–433.
5 Amor S, McNamara NB, Gerrits E, Marzin MC, Kooistra SM, Miron VE, *et al*. White matter microglia heterogeneity in the CNS. *Acta Neuropathol* 2022; **143**:125–141.
6 Xu S, Lu J, Shao A, Zhang JH, Zhang J. Glial cells: role of the immune response in ischemic stroke. *Front Immunol* 2020; **11**:294.
7 Koivisto A, Hukkanen M, Saarnilehto M, Chapman H, Kuokkanen K, Wei H, *et al*. Inhibiting TRPA1 ion channel reduces loss of cutaneous nerve fiber function in diabetic animals: sustained activation of the TRPA1 channel contributes to the pathogenesis of peripheral diabetic neuropathy. *Pharmacol Res* 2012; **65**:149–158.
8 Lee KI, Lin HC, Lee HT, Tsai FC, Lee TS. Loss of transient receptor potential ankyrin 1 channel deregulates emotion, learning and memory, cognition, and social behavior in mice. *Mol Neurobiol* 2017; **54**:3606–3617.
9 Shigetomi E, Jackson-Weaver O, Huckstepp RT, O'Dell TJ, Khakh BS. TRPA1 channels are regulators of astrocyte basal calcium levels and long-term potentiation via constitutive D-serine release. *J Neurosci* 2013; **33**:10143–10153.

10 Oh SJ, Lee JM, Kim HB, Lee J, Han S, Bae JY, *et al*. Ultrasonic neuromodulation via astrocytic TRPA1. *Curr Biol* 2019; **29**:3386–3401 e3388.
11 Corrigan F, Mander KA, Leonard AV, Vink R. Neurogenic inflammation after traumatic brain injury and its potentiation of classical inflammation. *J Neuroinflammation* 2016; **13**:264.
12 Kriszta G, Nemes B, Sandor Z, Acs P, Komoly S, Berente Z, *et al*. Investigation of cuprizone-induced demyelination in mGFAP-driven conditional transient receptor potential ankyrin 1 (TRPA1) receptor knockout mice. *Cells* 2019; **9**:81.
13 Hamilton NB, Kolodziejczyk K, Kougioumtzidou E, Attwell D. Proton-gated Ca2+-permeable TRP channels damage myelin in conditions mimicking ischaemia. *Nature* 2016; **529**:523–527.
14 Xia M, Chen W, Wang J, Yin Y, Guo C, Li C, *et al*. TRPA1 activation-induced myelin degradation plays a key role in motor dysfunction after intracerebral hemorrhage. *Front Mol Neurosci* 2019; **12**:98.
15 Krafft PR, Rolland WB, Duris K, Lekic T, Campbell A, Tang J, *et al*. Modeling intracerebral hemorrhage in mice: injection of autologous blood or bacterial collagenase. *J Vis Exp* 2012; **67**:e4289.
16 Chen W, Zheng P, Hong T, Wang Y, Liu N, He B, *et al*. Astrocytes-derived exosomes induce neuronal recovery after traumatic brain injury via delivering gap junction alpha 1-20 k. *J Tissue Eng Regen Med* 2020; **14**:412–423.
17 Chu X, Wu X, Feng H, Zhao H, Tan Y, Wang L, *et al*. Coupling between interleukin-1R1 and necrosome complex involves in hemin-induced neuronal necroptosis after intracranial hemorrhage. *Stroke* 2018; **49**:2473–2482.
18 Heindl S, Gesierich B, Benakis C, Llovera G, Duering M, Liesz A. Automated morphological analysis of microglia after stroke. *Front Cell Neurosci* 2018; **12**:106.
19 Sahraeian SME, Mohiyuddin M, Sebra R, Tilgner H, Afshar PT, Au KF, *et al*. Gaining comprehensive biological insight into the transcriptome by performing a broad-spectrum RNA-seq analysis. *Nat Commun* 2017; **8**:59.
20 Dragic M, Milicevic K, Adzic M, Stevanovic I, Ninkovic M, Grkovic I, *et al*. Trimethyltin increases intracellular Ca(2+) via L-type voltage-gated calcium channels and promotes inflammatory phenotype in rat astrocytes in vitro. *Mol Neurobiol* 2021; **58**:1792–1805.
21 Jha MK, Jo M, Kim JH, Suk K. Microglia-astrocyte crosstalk: an intimate molecular conversation. *Neuroscientist* 2019; **25**:227–240.
22 Yuan J, Liang X, Zhou W, Feng J, Wang Z, Shen S, *et al*. TRPA1 promotes cisplatin-induced nephrotoxicity through inflammation mediated by the MAPK/NF-κB signaling pathway. *Ann Transl Med* 2021; **9**:1578.
23 Chen W, Guo C, Huang S, Jia Z, Wang J, Zhong J, *et al*. MitoQ attenuates brain damage by polarizing microglia towards the M2 phenotype through inhibition of the NLRP3 inflammasome after ICH. *Pharmacol Res* 2020; **161**:105122.
24 Zhang Y, Lian L, Fu R, Liu J, Shan X, Jin Y, *et al*. Microglia: the hub of intercellular communication in ischemic stroke. *Front Cell Neurosci* 2022; **16**:889442.
25 Zhang D, Lu Z, Man J, Cui K, Fu X, Yu L, *et al*. Wnt-3a alleviates neuroinflammation after ischemic stroke by modulating the responses of microglia/macrophages and astrocytes. *Int Immunopharmacol* 2019; **75**:105760.
26 Yang J, Vitery MDC, Chen J, Osei-Owusu J, Chu J, Qiu Z. Glutamate-releasing SWELL1 channel in astrocytes modulates synaptic transmission and promotes brain damage in stroke. *Neuron* 2019; **102**:813–827.e6.